Tailoring the photophysical properties and excitonic radiative decay of soluble CdSe quantum dots by controlling the ratio of capping thiol ligand

Randa Mrad, Mélanie Poggi, Nassim Ben Brahim, Rafik Ben Chaâbane,
Michel Négrerie

HAL Id: hal-02114117

https://polytechnique.hal.science/hal-02114117

Submitted on 21 Oct 2021

Tailoring the photophysical properties and excitonic radiative decay of soluble CdSe quantum dots by controling the ratio of capping thiol ligand

Randa Mrad[a], Mélanie Poggi[b], Nassim Ben Brahim[a], Rafik Ben Chaâbane[a], Michel Negrerie[c,*]

[a]Laboratoire des Interfaces et Matériaux Avancés, Faculté des Sciences de Monastir, Boulevard de l'Environnement, 5019 Monastir, Tunisia.
[b]Laboratoire de Physique de la Matière Condensée, CNRS, Ecole Polytechnique, 91120 Palaiseau, France.
[c]Laboratoire d'Optique et Biosciences, INSERM, CNRS, Ecole Polytechnique, 91120 Palaiseau, France.

* Corresponding author   E-mail address: michel.negrerie@polytechnique.edu

ABSTRACT

We report the physical and photophysical properties of CdSe quantum dots capped with three different thiol compounds (thioglycolic acid, 3-mercaptopropionic acid, mercaptosuccinic acid) synthesized through a hydrothermal protocol. We calculated the true molecular weight and molar absorption coefficient of QDs from their diameter (not from any empirical relation) which are in the range 3.5 – 5.9 nm. The aqueous synthesis method ensures the insertion of the sulfur atoms of thiol ligands in the crystal CdSe cubic lattice, producing hexagonal crystal unit defects at the surface of the QDs. The QDs steady-state emission spectra were analyzed in terms of gaussian components, in correlation with the time-resolved emission. We have elaborated MSA-CdSe QDs capped with mercaptosuccinic acid using various stoichiometric Cd/MSA ratios during the aqueous synthesis. Modulating the Cd/MSA ratio directly affects the size and photophysics of the QDs, in particular the fluorescence emission spectrum and decay. We rationalized the effect on QDs size by a change of the CdSe formation rate during synthesis. Acting on the Cd/MSA ratio appears a mean of modulating the emission spectrum and understanding the photophysical processes involved with respect to the QD structure.

Keywords: CdSe quantum dots; Electronic microscopy; Quantum dots fluorescence; Surface state emission; Thiol capping ligands; CdSe/MSA stoichiometry

1. Introduction

Colloidal semiconductor nanocrystals or quantum dots (QDs) have particular photophysical properties due to their nanometer size and the subsequent quantum confinement effect [1]. The tunable size and optical properties of group II-VI semiconductor QDs offer a broad range of potential applications, especially in optoelectronics, photocatalysis, chemical sensing, light conversion and probes in biological sciences [2–11] and many protocols were designed to understand and control the influence of synthesis parameters on the QDs properties. Core/shell QDs were developped, providing another parameter for modulating the QDs photophysical properties [12,13] including their quantum yield, and may also overcome the possible leak of Cd, which is toxic for cells. Useful QDs are synthesized in solution in the presence of coordinating ligands that bind to the semiconductor surface and influence the nanocrystal nucleation and growth process. The syntheses can be classified, depending on the solvent used, as organic [12,14,15] or aqueous [2,16–18] which both offer the possibility of finely tuning the optical properties of QDs, especially the fluorescence emission, by the modification of their size through controled parameters, including surface functionalization [16,19–21].

The first syntheses of QDs were performed in organic solvents, [1] however, both pure core or core/shell QDs can be rendered water soluble by surrounding the semiconductor nanocrystals with a polar chain grafted to the crystal lattice [13–15]. Grafting of a soluble chain can be performed after the synthesis of QDs [22] or alternatively the ligand can be incorporated during the synthetis as a precursor [17,18]. Using a totally aqueous synthetic method, the soluble capping groups are directly grafted to the semiconductor material, provided that they possess an atom which can be inserted within the crystal phase. Usually thiol derivatives with a carboxylic function are employed, the sulfur being amenable to insertion in both CdS and CdSe lattices. The thiol reagent is present in the very first step of synthesis and both its nature and stoichiometry with respect to other reagents are expected to influence the properties of the prepared QDs. Here, we aimed at investigating how the nature and stoichiometry of thiol derivatives of carboxylic acids change the size and photophysical properties of CdSe QDs.

The ligand grafted around the semiconductor core plays an important role in binding to Cd atoms at the QD surface, thus interfacing the semiconductor lattice and the solvent. They change the atomic orbitals at the surface which could trap charge carriers and thus modify the electronic and photophysical properties of the nanocrystal [23–26]. Therefore, besides

ensuring the solubility of QDs in water, the grafting of ligands provides means to control the photophysics of QDs [2,16,19–21,27–31]. For example, the use of thiols coupled with charged or hydrophilic groups as capping agents allows to improve the fluorescence quantum efficiency of synthesized QDs [17] and mercaptopropionic acid (MPA) was shown to produce QDs with a large range of size and fluorescence tunability [17]. Another crucial parameter is the stoichiometric ratio of Cd atoms to the capping ligand, which may eventually changes all the QDs properties including size, structure and fluorescence. Knowing precisely the influence of capping ligands and synthesis parameters on the structural and optical properties of CdSe QDs allows one to choose the suitable conditions for the design of appropriate QDs for analytical or biomedical specific applications, especially for interaction with analytes.

Here, we analyzed the effects of changing two important parameters which influence the hydrothermal synthesis of water-soluble CdSe functionalized QDs, namely the nature of the surface thiol ligands and their stoichiometric ratio with respect to the precursors which provide Cd and Se atoms. The three ligands possess a thiol function for interaction with the CdSe lattice, but have varied organic chains (Scheme 1): thioglycolic acid (TGA), 3-mercaptopropionic acid (MPA) and mercaptosuccinic acid (MSA). To investigate the Cd/ligand stoichiometric ratio we have selected MSA as the capping ligand because it possesses two carboxylic acid groups making it an attractive probe for numerous molecular interaction studies in solution. The amount of thiol provided during the synthesis is addressed here, not the concentration of thiols in the solution once the QDs are synthesized [31]. We synthesized by an aqueous route four kinds of hydrophilic MSA-CdSe QDs which only differ in the molar ratio Cd/Se/MSA, set between 1/0.5/1 and 1/0.5/2.5 and keeping constant the Cd/Se ratio for ensuring the semiconductor crystal growth. We evaluated the effects of varying the nature of ligand and the stoichiometric ratio on in the QDs physical properties probed by X-ray diffraction, high-resolution electron microscopy and IR, while their optical properties were probed by UV–vis absorption, steady-state and time-resolved fluorescence spectroscopies. Overall, whereas the nature of the thiol-containing capping ligand does not affect the structure of synthesized CdSe QDs, their optical properties can be modulated. Contrastingly, changing the stoichiometric ratio Cd/Se/MSA largely influences both the QDs size and their photophysics through a change of the relative amplitudes of the band edge and trap state emissions.

Thioglycolic Acid   Mercaptopropionic Acid   Mercaptosuccinic Acid
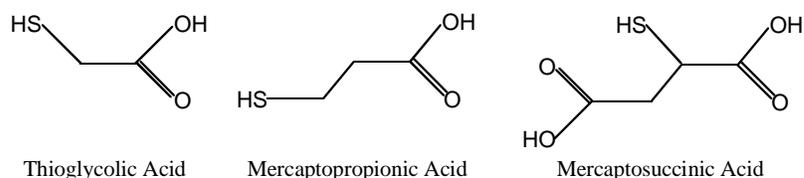
Scheme 1. Molecular structures of the thiol ligands for surface capping of CdSe QDs.

2. Experimental section

2.1. Chemicals

Cadmium acetate dehydrate (Cd (CH$_3$COO)$_2$·2H$_2$O, 98%, Sigma-Aldrich) and selenium dioxide powder (SeO$_2$, 98%, Aldrich) were used as cadmium and selenium sources. Sodium borohydride (NaBH$_4$, 98%, Aldrich) was used as the reducing agent. Thioglycolic acid (TGA, C$_2$H$_4$O$_2$S), 3-mercaptopropionic acid (MPA, C$_3$H$_6$O$_2$S) and mercaptosuccinic acid (MSA, C$_4$H$_6$O$_4$S, 97%) from Sigma-Aldrich were successively used as capping ligands (Scheme 1). Sodium hydroxide (NaOH, Spectrochem) allowed to control the pH. Distilled water was used as the solvent for all steps of the CdSe QDs synthesis. All chemical were used as purchased without further purification.

2.2. Synthesis of water soluble CdSe nanocrystals with different ligands

The colloidal CdSe QDs capped with three ligands MPA, TGA and MSA were prepared based on the aqueous method described elsewhere [18,32], with some modification (Fig. 1). Briefly, an aqueous colorless solution was obtained by mixing cadmium acetate dehydrate with either TGA, MPA or MSA as the stabilizer in deionized water with continuous stirring under nitrogen atmosphere. The pH of the solution was adjusted to 11 by dropwise addition of 1.0 M NaOH solution with stirring to solubilize the Cd^{2+}–ligand complex. Separately, an aqueous solution of Na$_2$SeO$_3$ was prepared by introducing SeO$_2$ into a NaOH solution and injected into the mixture of Cd^{2+} and ligand under vigorous stirring at room temperature. The molar ratio of Cd/Se/XA was set at 1/0.5/1.7 when comparing the ligands TGA, MSA and MPA. When investigating the influence of the molar ratio of Cd/Se/MSA, it was set at 1/0.5/1, 1/0.5/1.5, 1/0.5/2 and 1/0.5/2.5, the only varying parameter, keeping constant the Cd/Se ratio. Then, a solution of the reducing agent NaBH$_4$ was added with a syringe into the final solution with continuous stirring at 100 °C under N$_2$ until the solution became light yellow. This color change indicates that the XA-capped CdSe QDs were obtained. Finally, the precipitate was isolated from unreacted reagents by centrifugation, washed with methanol

several times and further dried in a desiccator under vacuum. All QDs were stored as powder in the dark at 20 °C and were dissolved in deionized water immediately before use.
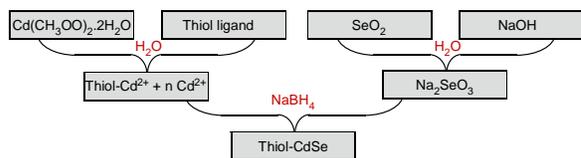

Fig. 1. Summary of the main steps for the synthesis of the capped CdSe nanoparticles. Thiol ligand formulas are given in Scheme 1.

2.3. Structural characterization

The X-ray diffraction (XRD) pattern of powder samples was collected using a XPERT PRO MPD panalytical powder X-ray diffractometer with a nickel-filtered K_α radiation from Cu (λ = 1.541 Å) in the 2θ range of 10° – 80° at room temperature. The XRD data were analyzed using JCPDS software. The FTIR spectra was measured on a Perkin Elmer Fourier transform infrared spectrophotometer at room-temperature with the samples grounded in KBr wafer. The Raman spectrum was recorded with a LABRAM HR-Raman spectrometer (HORIBA, Jobin-Yvon). The excitation wavelength from an Argon ion laser (568 nm) is located outside any absorption band of the QDs, to ensure that fluorescence was negligible.

For recording high-resolution transmission electron microscopy (HRTEM) images, we employed a JEOL 2010 FEG with an accelerating voltage of 200 kV. The samples were prepared by dropping the QDs dispersed in water onto carbon-coated copper grids and the excess solvent was evaporated. Zeta potential and dynamic light scattering measurements were performed using a Malvern Zetasizer-NanoZS instrument.

2.4. Photophysical characterization

The UV–visible absorption spectra were obtained on a Shimadzu UV-1700 spectrophotometer with a 1-cm optical path quartz cuvette. The steady-state fluorescence measurements were carried out on a Cary Eclipse spectrometer with the sample in a 1-cm optical path quartz cuvette and with an excitation at 350 nm. The slit width was 10 nm for both the excitation and emission. A 2-mm thick 385-nm cut-off filter (Schott) was placed before the emission entrance slit to block possible scattered excitation light and avoid its diffracted second order at 700 nm. For quantum yield measurements, fluorescein excited at 350 nm was used as the standard. The fluorescence lifetimes were measured with a Horiba Fluorolog system using an excitation wavelength at 372 nm provided by a NanoLED

(Horiba). All optical measurements were carried out at room temperature. For spectroscopic measurements the concentration of QDs was in the range $1 - 3$ mg·mL^{-1}.

Fluorescence quantum yields were calculated using fluorescein (Sigma, ref. 6377) dissolved in water at pH = 11 (0.1 M NaOH) as a standard of quantum yield $\Phi_{Fr} = 0.89$, measuring the emissions by always exciting at the same excitation wavelength (350 nm) as used for CdSe QDs. The emission wavelength range $400 - 800$ nm was the same for all CdSe QDs samples. The UV absorption and fluorescence spectra of fluorescein and CdSe QDs in water were recorded successively with exactly the same conditions. The fluorescence quantum yield Φ_{QD} was calculated using the protocol proposed by Würth et al. [33] using the equation:

$$\Phi_{QDs} = \Phi_{Fr} \frac{F_{QDs}}{F_{Fr}} \frac{I_{Fr}^{Abs}}{I_{QDs}^{Abs}} \frac{F_{Fr}^{i}(\lambda_{ex}, \lambda_{em})}{F_{QDs}^{i}(\lambda_{ex}, \lambda_{em})}$$

(1)

where, $I^{Abs}(x) = 1 - 10^{-Ax}$, A_X is the absorbance of the sample x at the excitation wavelength, F_{QD} and F_{Fr} are the integrated fluorescence intensity of the QDs and the reference sample respectively. $I_{QD}{}^{Abs}$ and $I_{Fr}{}^{Abs}$ are the fractions of absorbed excitation light at the wavelength used to record the fluorescence emission. $F^{i}(\lambda_{ex}, \lambda_{em})$ is the instrument function comprising the spectral profile of the excitation and the response of the optics and detector of the fluorescence spectrometer, within the spectral range of the sample. Since we have used the same excitation wavelength and exactly the same cells, settings and parameters for both samples, the instrument function is the same for both samples.

3. Results and discussion

3.1. Structural and chemical characterization

3.1.1. Structure and size

HRTEM allowed us to simultaneously verify the crystal structure and shape and measure the size of the functionalized CdSe QDs. The HRTEM images of TGA-CdSe, MPA-CdSe and MSA-CdSe QDs (Fig. 2 and Fig. S1 in Supplementary data file) confirmed that the shapes of these CdSe QDs are nearly spherical and have a distribution of average diameters centered at 3.6 ± 0.2 nm, 4.3 ± 0.2 nm and 4.0 ± 0.2 nm for TGA-, MPA- and MSA-CdSe QDs, respectively. The similar particle lattice and sizes measured indicated that the hydrothermal synthesis is not affected by the nature of the capping thiol molecules. The lattice plane spacing of $0.34 - 0.35$ nm corresponds to the (111) diffraction plane of the cubic phase

of CdSe [29–30] and confirms the good crystalinity of these QDs. The diameters measured by HRTEM correspond to the crystal core size and are expected to be smaller than the hydrodynamic diameter of the QDs [34]. The measurement of diameters by dynamic light scattering (DLS) (Fig. S2) revealed the same size evolution as a function of the capping ligand, all diameter being slightly larger than those obtained from HRTEM images, because of the presence of the grafted ligand (Table 1).
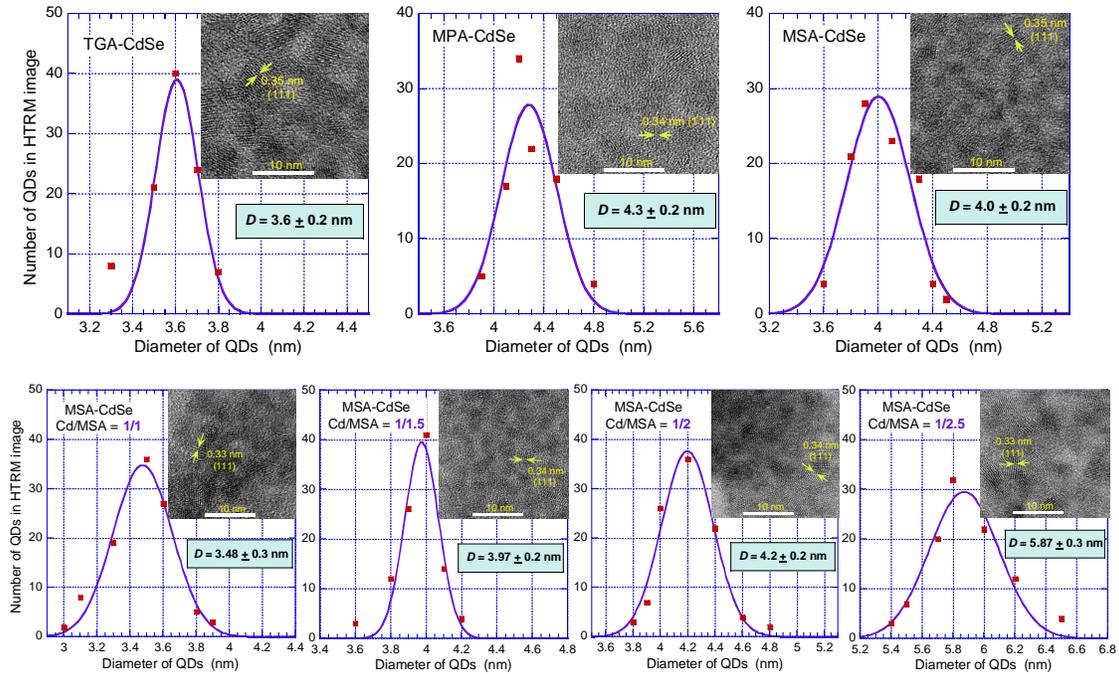

Fig. 2. Gaussian distribution of the size of various synthesized CdSe QDs, with different thiol ligands and different Cd/MSA ratios, determined from invidual measures of n = 100 QDs. The insets show the corresponding HRTEM images of CdSe nanocrystals with distinct lattice fringes appearing in one or more directions.

Changing the Cd/MSA molar ratio does not alter the spherical morphology of the synthesized CdSe QDs (Fig. 2). Remarkably, their diameter, determined from the Gaussian distribution of 100 QDs, increased gradually from 3.5 to 5.86 nm when varying the Cd/MSA from 1:1 to 1:2.5 (these diameters, determined from TEM measurements, do not correspond to the hydrodynamic sizes, which take also into account the grafted ligands). This size evolution have consequences toward the QDs photophysics due to the confinement effect (see below). The lattice spacing of 0.33 ± 0.01 nm corresponds to the (111) diffraction plane of cubic phase and demonstrates that the crystal phase is not affected by the Cd/MSA stoichiometric ratio in the range 1/1 – 1/2.5. It appears that this ratio is more important in determining the size than the nature of the thiol ligand.

The crystallinity of all synthesized CdSe QDs was also verified by recording X-ray diffraction spectra (Fig. 3), noting that CdSe can exist both in cubic or hexagonal phases [2]. The peak positions for CdSe-TGA (29.27°, 41.35°, 48.67°), CdSe-MPA (27.49°, 42.79°, 50.30°) and CdSe-MSA (27.73°, 42.76°, 48.85°) correspond to the crystallographic planes (111), (220) and (311) of the cubic crystal structure of CdSe (JCPDS card No. 00-19-0191), in agreement with the lattice interplanar distance of 0.34 ± 0.01 nm determined by HRTEM assigned to the (111) plane of cubic blend structure of CdSe [35]. When changing the Cd/MSA stoichiometric ratio from 1/1 to 1/2.5 during synthesis, similar diffraction patterns are obtained, which indicate that the crystal structure of CdSe particles is not altered. However, all XRD spectra contain also a contribution from the hexagonal phase since neither pure cubic phase, nor pure hexagonal phase can perfectly account for the observed data. A Rietveld analysis performed to determine the line breadth turned out to be difficult due to the entangled and broad peaks and yielded large uncertainties, so that the use of Sherrer's equation [36] led to underevaluating the diameters (in the range 1.8 – 2.5 nm) with respect to statistics from TEM images. For exemple the diffraction peak from the (220) plane of cubic phase appears at same angle as the (110) hexagonal contribution, whereas the hexagonal (100) peak does not contribute (or in small proportion) and the (311) contributes mostly in TGA and MPA-CdSe spectra. The most predominant phase of these CdSe QDs is cubic but the contribution from hexagonal structure is certain. The broadening of the diffraction peaks proves the small size of the nanoparticles, which thus possess a large number of crystal units at the surface with respect to the QD core, favoring surface defects and mixed structure, as it will be discussed after analysis of the fluorescence spectra. We rationalized that the grafting of the thiol ligands occurred through a Cd–S bond, favoring hexagonal crystal units and surface defects due to insertion of S atoms in place of Se atoms, as seen below. Overall, these data (Table 1) show that changing the nature of the thiol capping ligand, or increasing the MSA amount do not alter the crystal structure of the CdSe QDs, albeit in all QDs there exits a variable proportion of crystal units in hexagonal phase. The nature of the thiol ligand influences the diameter, as observed for carboxylic acid precursors in organic synthesis [37], albeit their respective final roles are different.
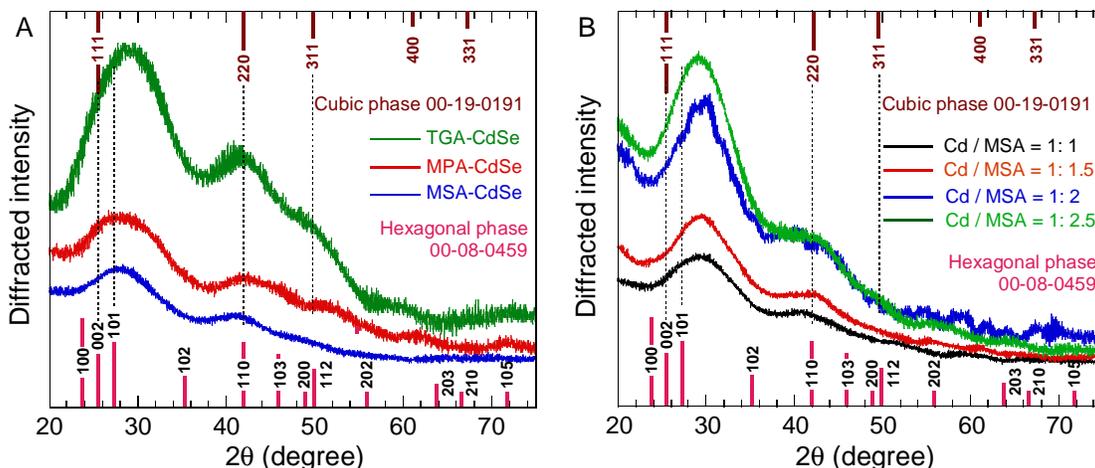
Fig. 3. X-ray diffraction spectra of CdSe QDs capped with three thiol ligands (A) and with different Cd/MSA ratios in the range 1/1 – 1/2.5 (B). The diffraction patterns of cubic and hexagonal phases for bulk CdSe are indicated (from Joint Committee on Powder Diffraction Standards).

We rationalized the increase of the CdSe-MSA QDs diameter (Table 1) when changing the Cd/MSA ratio from 1/1 to 1/2.5 during synthesis by a change of the kinetic rates. One must note that the intermediate compound $R–S–Cd^{2+}$ is first formed from MSA and Cd acetate (Fig. 1) and its concentration is thus increased, but does not deplete free Cd in the reacting solution as we used a ratio Cd/Se = 1/0.5. Importantly, because MSA is grafted to Cd before reacting at the QD surface, MSA insertion and crystal growth are simultaneous processes. The increase of $R–S–Cd^{2+}$ concentration does not induce a faster termination of the reaction by saturating the possible binding sites, but rather stabilizes QDs and facilitates their growth (n Cd + m Se → CdSe-QD) by slowing down the release of Cd^{2+} and Se^{2-} atoms from the already formed lattice. Thus, the kinetic rate of the reverse reaction CdSe-QD → n Cd + m Se is slowed down. Our interpretation is in agreement with a study on CdSe nanocrystals synthesis whose authors noted that "quantum dot syntheses are highly susceptible to small variations in precursor preparation" [38]. This behavior is also reminiscent of the similar observation of increased diameter of CdSe QDs capped with octadecene when increasing the ODE-Se precursor concentration during the organic synthesis [15].

3.1.2. Functionalization and chemical composition

In order to ascertain the binding of the thiol ligands to the surface of CdSe nanoparticles we have recorded FTIR spectra of all synthesized QDs in the solid state (Fig. S3). The presence of bound thiols is confirmed by the absorption bands at 1225, 2920, 667 and 1211 cm^{-1}, assigned to the stretching vibrations of C–O bond and C–H, C–S and C–O bonds,

respectively [39]. The carboxylic acid group COO^- produces the symmetric and asymmetric vibrations at 1401 cm^{-1} and 1567 cm^{-1}. Importantly, the absence of S–H stretching bands around 2560 cm^{-1} indicates that S atoms no longer form thiol groups but are bound to the surface of CdSe nanoparticles through Cd–S ligation, a hypothesis to be verified by Raman spectroscopy. The replacement of Se atoms with S atoms at the surface of the crystal structure is the reason why a pure cubic structure is not observed in the XRD spectra of capped QDs, but rather a mixed hexagonal/cubic one.

Any effect which impacts the crystal structure also impacts the vibrational modes of the lattice (phonons), an effect which is significant in the case of nanomaterials and observed by Raman scattering for CdSe, CdS and CdTe [40–45]. The Raman spectra of our CdSe QDs capped with thiol ligands display two main bands (Fig. S4). The first one (centered at 200 cm^{-1} for TGA-CdSe, 205 cm^{-1} for MSA-CdSe and 210 cm^{-1} for MPA-CdSe), corresponds to the first-order longitudinal optical phonon (1LO) mode of CdSe [41]. The second one (centered at 292, 295 and 287 cm^{-1} for TGA-CdSe, MPA-CdSe and MSA-CdSe QDs, respectively) is assigned to the 1LO phonon mode of CdS [42,44,45]. The LO phonon bands are broader for QDs than for bulk CdSe. The intensity of the first 1LO phonon band is much weaker for MPA- compared to TGA- and MSA-CdSe QDs, due to a less ordered cubic structure, in line with the broader band from the (111) plane in the XRD diffraction spectrum of MPA-CdSe (Fig. 3). The surface optical mode SO is merged with the longitudinal optical 1LO, the former being observed in nanoparticles due to their larger surface to volume ratio than in bulk material [46], leading to an asymmetric band (185 – 205 cm^{-1}). The transverse optical mode TO [47–49] can only be seen as a weak band at ~160 cm^{-1}. The important observation is the simultaneous presence of the 1LO phonon modes from both CdS and CdSe, which implies that the grafting of thiol ligands to CdSe nanoparticles involves Cd–S chemical bonds inserted in the crystal lattice, as hypothesized from the synthesis route and from the XRD and IR spectra. The measurement of 1LO phonon modes simultaneously from both compounds have also been reported in the case of core/shell [44] and core/crown CdSe/CdS nanoparticles [45].

The physical properties and stability of functionalized nanoparticles in aqueous phase are especially dependent on the electrical and ionic structure of the nanoparticle–liquid interface [50–52]. The zeta potential, which reflects the intensity of repulsive forces among QDs and consequently the stability of the colloidal dispersion, depends on the chemical composition of ligands at the particle surfaces and on the composition of the solvent [53–55]. The zeta potential of the synthesized QDs in water at pH = 7.4 (Fig. S5) (–21.3 mV for TGA-CdSe, –27.6 mV for MPA-CdSe and –28.9 mV for MSA-CdSe) indicates that the outer

surface layers are negatively charged due to the carboxylic acid groups, confirming the binding of the ligands. The zeta potential close to –30 mV allows a stable suspension in water [56] as it was observed in all experiments.

3.2. Optical properties

3.2.1. Absorption spectrum

It is well established that the optical properties of semiconductor nanoparticles, absorption, emission and quantum yield, depend upon their size [1,2,57] which determines their band gap energy. A variety of approaches have been considered to control the growth of particles of desired size [2,13,14,37,38]. Here, we evaluated the effects of the Cd/MSA molar ratio during synthesis on the properties of CdSe QDs. Increasing the Cd/MSA ratio from 1:1 to 1:2.5 shifts to longer wavelengths the absorption maxima and λ_{edge} of the first excitonic band (Fig. 4B), in agreement with the size evolution observed by HRTEM (Table 1).
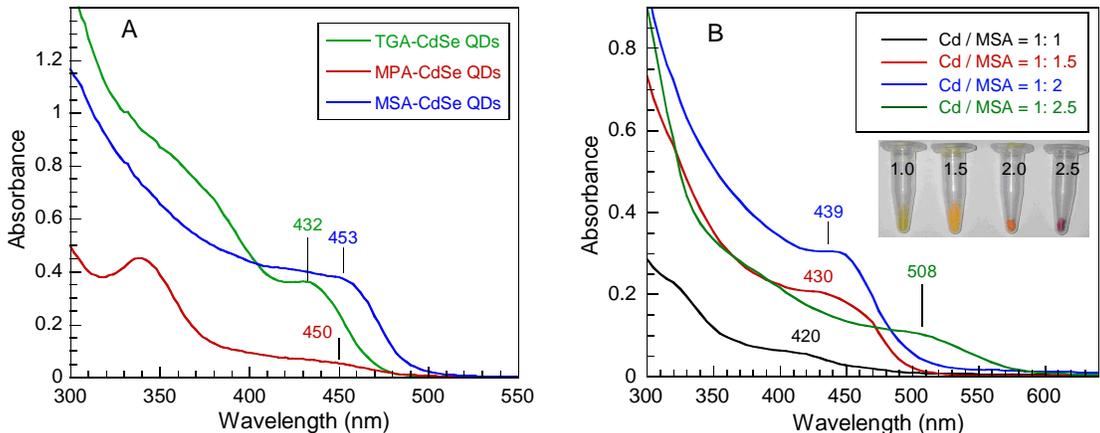

Fig. 4. Electronic absorbance spectra of CdSe QDs synthesized with different capping ligands (**A**) and with different Cd/MSA ratios (**B**). [QDs] = 0.05 mg·mL^{-1} for TGA- and MPA-CdSe. [QDs] = 0.05 to 0.15 mg·mL^{-1} for MSA-CdSe. Optical pathlength = 1 cm. T = 20 °C.

All the ligand-stabilized QDs show characteristic absorption bands due to the first excitonic transition (1Se – 1Sh) [58] and the absorption edges (λ_{edge}), which are located at 432, 450 and 453 nm for TGA, MPA- and MSA-CdSe QDs respectively, are shifted to higher values as a consequence of the size confinement effect (Fig. 4A). For TGA- and MPA-CdSe higher energy transitions are observed. The band gap energy of CdSe QDs was estimated in order to further confirm the accuracy of sizes measured by HRTEM. According to the relation $\varepsilon h\nu = A (h\nu - E_g)^n$ (where ε is the absorption coefficient, A a constant, $h\nu$ the photon energy

and n = 1/2 is a constant for direct semiconductors) the band gap energy was obtained from the variation of $(\varepsilon h\nu)^2$ as a function of hν (Fig. S6 and Table 1). The decrease of the band gap energy measured for Cd/MSA ratio from 1:1 to 1:2.5 originates from the weaker quantum confinement effect due to increasing particle size.

The molar absorption coefficient is a very important parameter. Rather than to estimate it from an empirical relationship [59], we calculated it from the absorbance at the maximum of band edge and the molecular weight $MW_{(QD)}$, which was obtained from the individual QD size [60–62]. Briefly, we calculted the absolute number of Cd and Se atoms in one QD using its diameter and the volume of a crystal unit. We calculated the number of crystal units exposed to the surface and assumed that one thiol-Cd^{2+} precursor is inserted in each unit at the surface, replacing a Se atom, an assumption which was verified in the case of thioglycerol-CdS QDs [60] (see Supplementary Information file for details). All values are listed in Table 1. The absorption coefficients of the three TGA-, MPA- and MSA-capped QDs agree with the curve determined for nanocrystals prepared through organic synthesis [63].

Table 1. Physical characteristics of the various QDs as a function of synthesis conditions.

QDs (a)	D_{TEM} (nm)	D_{DLS} (nm) (b)	$MW_{(QD)}$ (g·mol^{-1})	ε (c) (M^{-1}·cm^{-1})	λ_{Edge} (nm)	λ_{em} (nm)	Φ_{QD} (%) (d)	E_g (eV)
TGA-CdSe	3.6 ± 0.2	5.0 ± 0.2	0.94×10^5	1.8×10^5	432	479, 608	0.13	2.80
MPA-CdSe	4.3 ± 0.2	5.8 ± 0.6	1.50×10^5	1.4×10^5	450	585	1.80	2.61
MSA-CdSe	4.0 ± 0.2	4.6 ± 0.2	1.30×10^5	1.5×10^5	453	550	5.61	2.41
$R_1 = 1.0$	3.5 ± 0.1	-	0.90×10^5	1.0×10^5	420	505, 615	0.48	2.50
$R_2 = 1.5$	4.0 ± 0.1	-	1.27×10^5	8.0×10^5	430	550	7.08	2.40
$R_3 = 2.0$	4.2 ± 0.1	-	1.47×10^5	15×10^5	439	554	5.93	2.25
$R_4 = 2.5$	5.9 ± 0.2	-	3.75×10^5	14×10^5	508	580	0.29	2.02

(*a*) R_i represent the MSA/Cd stoichiometric ratio during the synthesis of MSA-CdSe.
(*b*) From dynamic light scattering measurements.
(*c*) Absorption coefficient at the maximum λ_{Edge} of the first excitonic band.
(*d*) Quantum yield at the maximum of emission spectrum (Fig. S7).

3.2.2. Emission spectrum

The room temperature fluorescence spectra of CdSe nanoparticles in solution capped with the three thiols TGA, MPA and MSA (Fig 5A) show a major band of higher intensity centered at 608, 585 and 550 nm, respectively. The displacement of this main band toward larger energy as a function of ligands does not follow the trend of the absorption band edge (Fig. 4A). We infer that the ligands differently influence the Stokes shift, and consequently the energy levels for exciton recombination, which is not solely determined by the CdSe QD size, as observed for exemple in CdTe [17]. The three fluorescence spectra possess also a

shoulder located at ~703 nm, which is reduced when MSA is the capping ligand. They also differ markedly on their high energy side. A pronounced shoulder at 479 nm is present in the spectrum of TGA-CdSe, but the spectrum of MSA-CdSe has an abrupt rise, contrastingly to that of MPA-CdSe. To distinguish the differences in the origin of fluorescence emission between QDs, we have decomposed each emission spectrum in several bands which were assumed to have a gaussian profile (Fig. 5B, C and D). For all thiol ligands, the spectra disclose three bands, a major one and two minor bands on the lower and larger energy sides, which have different relative intensity ratios (Table 2). Whereas the band at 475 nm appears higher than at 720 nm for TGA-CdSe, the ratio is inverted for MPA-CdSe. Contrastingly, the counterpart bands are located much closer in the case of MSA-CdSe (517, 570 and 638 nm) with larger amplitude for the side emission bands (Fig. 5D). This effect may be attributed to the presence of two carboxylic groups, compared to only one for TGA and MPA (Scheme 1).
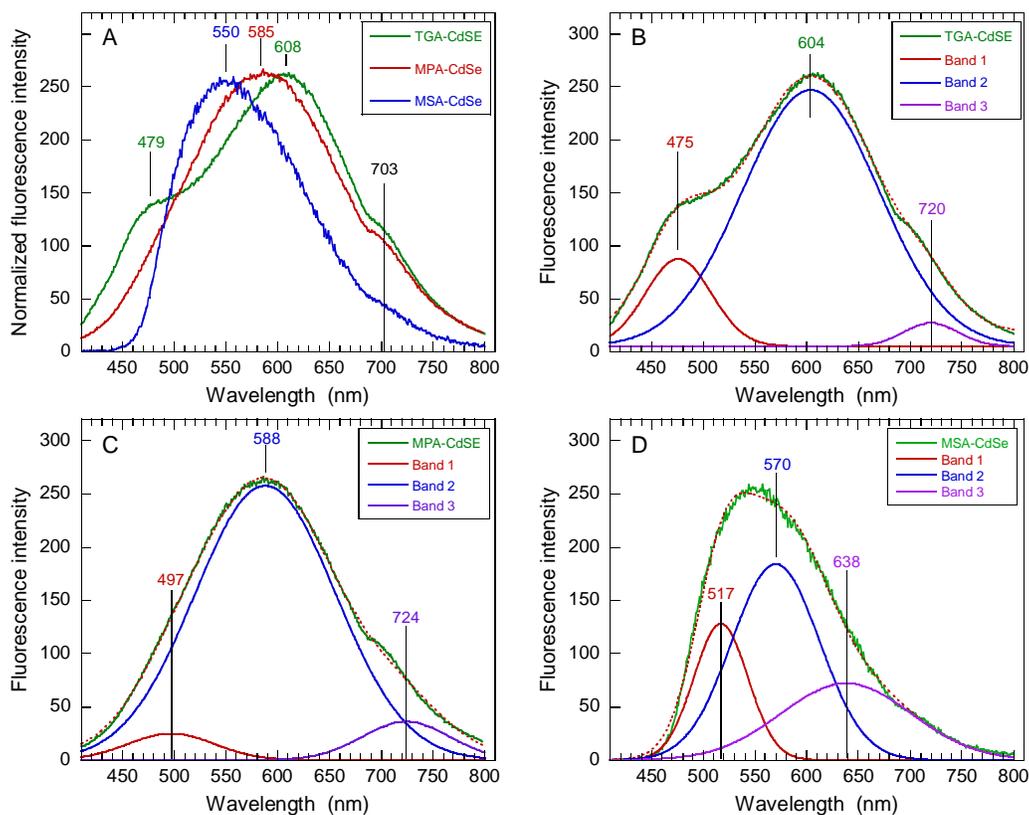

Fig. 5. Fluorescence emission spectra of TGA-, MPA- and MSA-CdSe QDs synthesized with different capping ligands (**A**). λ_{ex} = 350 nm. [QDs] = 0.05 mg·mL^{-1}. Optical pathlength = 1 cm. T = 20 °C. The three spectra of CdSe QDs were fitted to the sum of three gaussian functions (**B**, **C** and **D**). The red dotted line is the result of the fit.

The pH influences the optical properties of functionalized CdSe QDs. When increasing the pH from 6.5 to 10.5, the fluorescence intensity of the QDs globally decreased (Fig. S8) with a maximum at pH 9 for MPA-CdSe followed by a decay. Since the measurement was performed at pH above the pK_a of the ligand carboxylates (3.7, 4.34 and 3.49 respectively for TGA, MPA and MSA) the hypothesized origin of this pH dependence is the existence of secondary coordinations between the carboxyl oxygen and cadmium [64] which influence the surface states.

The dependence of the emission spectrum upon the Cd/MSA ratio was similarly analyzed and appeared very contrasted (Fig. 6 and Table 2) and. At a ratio of 1:1, the higher energy band is prominent at 505 nm, whereas the broader main band appears at 615 nm together with a shoulder at 703 nm. Fitting the spectra to a sum of gaussian emission bands yielded a major band and two minor ones, whose relative intensity evolves as a function of the Cd/MSA ratio (Table 2). The emission spectrum could be satisfactorily fitted with a sum of two gaussian bands only in the case of Cd/MSA ratio = 2.5 (Fig. 6E), with the possibility that two very close bands are merged into a large one, but that we could not separate.
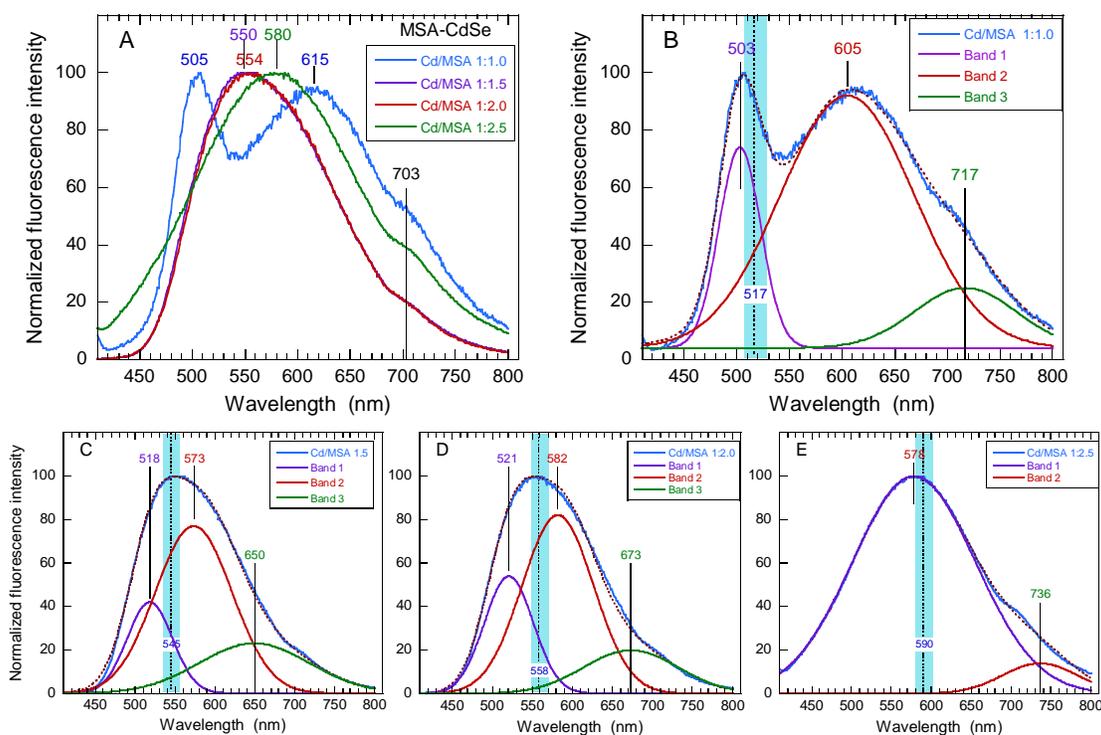

Fig. 6. Fluorescence emission spectra of MSA-CdSe QDs synthesized with different Cd/MSA ratios (**A**). λ_{ex} = 350 nm. [QDs] = 0.05 to 0.15 mg·mL^{-1}. Optical pathlength = 1 cm. T = 20 °C. The four spectra of MSA-CdSe QDs were fitted to the sum of three (**B**, **C** and **D**) or two (**E**) gaussian functions.

The red dotted line is the result of the fit. The vertical blue band is the spectral range of emission (25 nm) used to record the fluorescence decays (Fig. 7) at the indicated particular wavelengths.

The three components must now be assigned. Similarly with the spectra of various thiol ligand-QDs (Fig. 5) the second emission band has always the larger relative amplitude, a characteristic which does not necessarily implies its identification as the band edge emission from the core (examples for thiol-CdSe in Ref. [65] and [66]). For identifying the band edge emission, we followed the rule of its dependence with the MSA-CdSe QDs size [59,67] with same capping ligand, which is parallel to the dependence of the first excitonic absorption peak with the size [59,67]. Thus, assignment of the higher energy gaussian component 1 as the core emission was ascertained because its wavelength central position increases as a function of the CdSe QDs size (Table 2). Indeed, for CdSe the emission maximum moves linearly toward lower wavelength (with increasing difference between conduction and valence bands) as the edge absorption maximum decreases, until the conduction band reachs the fixed energy level of a surface state where excited electrons are promoted [67]. It follows that bands 2 and 3 are due to emission involving surface trap defects and that two different trapping processes take place (which can involve both shallow and deep trap defects), probably due to Se vacancies and hole interaction with S atoms from thiols [65]. Knowing their exact nature and identifying the relaxation pathways would require time-resolved absorption measurements.

Table 2. Parameters of the gaussian fits of fluorescence spectra of the various CdSe QDs.

QDs (a)	size (nm)	Component 1			Component 2			Component 3		
		position (nm)	*height* %	width (nm)	position (nm)	*height* %	width (nm)	position (nm)	*height* %	width (nm)
TGA-CdSe	3.6	475	*24*	46	604	*70*	93	720	*6*	37
MPA-CdSe	4.2	497	*8*	59	588	*81*	96	724	*11*	60
MSA-CdSe	3.9	517	*33*	37	570	*48*	60	638	*19*	89
$R_1 = 1.0$	3.5	503	*39*	27.7	605	*49*	89.5	717	*12*	66.8
$R_2 = 1.5$	3.8	518	*30*	40.4	573	*54*	68	650	*16*	98.4
$R_3 = 2.0$	4.2	521	*34*	43	582	*53*	62.6	673	*13*	83
$R_4 = 2.5$	5.9	578	*88*	109	–	–	–	736	*12*	66.5

(a) R_i represent the Cd/MSA stoichiometric ratio during the synthesis of MSA-CdSe.

The fluorescence band 1 of higher energy (475 – 521 nm) arises from band edge emission due to direct exciton recombination in the core of the semiconductor CdSe QDs, similarly to CdSe capped with mercaptoethanol [65] or other thiols derivatives [18,61,60]. The lower energy emission (638 – 724 nm) is assigned to defects localized in crystal units at the surface of nanocrystals (surface emission or "trap states") [68,69] which originate from

non stoichiometric bonds. Observation of two lower energy bands in the emission spectrum is not unique, and was also reported for thioglycerol-CdSe, assigned to deep trap defects [70] and for MPA-CdSe in which the concentration of MPA changed the amplitude ratio between band edge and trap state emissions [71]. In CdSe, defects generally consist of deficiencies of either cadmium or selenium, interstitial selenium which may acts as donor and surface adsorbed cadmium atoms [72,73]. Defects are favored by the coexistence of both cubic and hexagonal units in the CdSe lattice. Emission bands from trap states having a larger amplitude than that from band edge emission were also observed in the case of small size (3.1 – 3.3 nm) CdS [74] and MPA-CdSe QDs [59] with well separated emission bands. In the case of CdS [74] the relative amplitude of emission from core exciton recombination (band edge) and trap states is highly sensitive to the QD size, and the emission band from trap states has always a larger bandwidth than the band edge emission, as observed here.

The behavior of the fluorescence emission bands was further evaluated by time-resolved spectroscopy. The fluorescence decays for CdSe nanocrystals with different ligands or Cd/MSA ratios were measured at the maximum of their fluorescence emission (Fig. 7). In the case of increasing Cd/MSA ratios, probing at these particular wavelengths allowed to overlap the band edge and trap state emissions (Fig. 6) to reveal their relative contributions. All decays were fitted using a biexponential function:

$$I_{FL}(t) = \alpha_1 \exp(-t/\tau_1) + \alpha_2 \exp(-t/\tau_2) + cst \tag{2}$$

and the average lifetimes τ_{AV} were calculated from as the fitted parameters (Table 3):

$$\tau_{AV} = \sum_i \alpha_i \tau_i^2 / \sum_i \alpha_i \tau_i \tag{3}$$
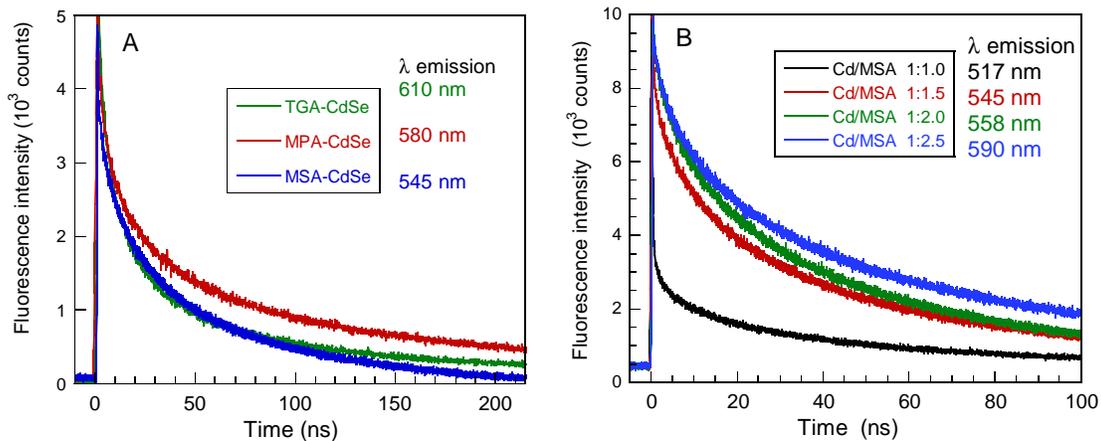

Fig. 7. Time-resolved fluorescence decays of CdSe QDs synthetized with different thiol ligands (**A**) and with different Cd/MSA ratios (**B**). Decays were recorded at the indicated emission maxima. Excitation wavelength λ_{ex} = 372 nm. Optical pathlength = 1 cm. The slit width for the emission was set at 25 nm (see Fig. 6).

Table 3. Fitted parameters of the fluorescence decays using a biexponential decay function.

QDs (a)	λ_{em} (nm)	α_1 (%)	τ_1 (ns)	α_2 (%)	τ_2 (ns)	τ_{AV} (ns)
TGA-CdSe	610	*70*	10.4	*30*	108	90
MPA-CdSe	580	*60*	12.0	*40*	137	122
MSA $R_1 = 1.0$	517	*49*	3.0	*50*	51	48
MSA $R_2 = 1.5$	545	*42*	6.7	*58*	58	54
MSA $R_3 = 2.0$	558	*41*	8.9	*59*	63	58
MSA $R_4 = 2.5$	590	*38*	8.5	*62*	70	66

(a) R_i represent the Cd/MSA stoichiometric ratio during the synthesis of MSA-CdSe.

The fluorescence emission of CdSe-QDs with three thiol capping molecules showed somewhat different decay profiles (Fig. 7A). The differences may arise here from both the varying size, as observed for CdS [74], and from influence of the nature of thiol ligands, as observed for 3-nm CdSe QDs [75], although in this latter case the high temperature synthesis in phosphonic acid may enhance the influence of thiol ligands. Contrastingly, TGA- and MPA-capped CdTe QDs (aqueous synthesis) of same size (2.3 nm) were shown to exhibit exactly the same decay parameters [17] while the dependence of decays with size is much stronger for MPA- than for TGA-CdTe QDs [17]. In the case of our three thiol-CdSe QDs, the size effect should be prominent. However, the average lifetimes observed in MSA-capped CdSe are shorter than those for TGA- and MPA-CdSe QDs (Table 3). The two carboxylic groups in MSA (Fig. 1) may participate in a more efficient excitonic relaxation, in particular by forming a secondary coordination between its COO^- and a Cd^{2+} atom, as suggested for CdTe [76] capped with TGA, MPA and MSA, which possess different ability to form secondary coordinations during synthesis of one-dimensional nanocrystals [76,77].

In MSA-CdSe QDs, we have probed the fluorescence decays at the maximum of emission (Fig. 7B) and it appears that the contribution from trap states emission varies in these conditions (Fig. 6B-E). Fitting these decays with a biexponential function results in the decrease of the amplitude α_1 of the shorter component τ_1 with concomitant increase of α_2. This trend follows the increasing proportion of surface trap states being probed at these particular wavelengths, as described for spectra (Fig. 6), and allowed us to assign the shorter decay component τ_1 to the direct recombination of excitons to the fundamental core state, whereas the longer component τ_2 is assigned to non-radiative e^-/h^+ recombination at the defect sites on the CdSe surface. Once the charge carriers have been trapped by the surface states, the radiative lifetime can be modulated (depending on the overlap of electron and hole wave functions), a process which depends upon the QD size [78,79]. Our assignment is in line with

an earlier interpretation based on the size-dependence of the emission in CdSe synthesized via an organometallic route [79] and water-soluble glutathione-capped ZnSe QDs [80] which disclose a relative amplitude of surface state emission in the same range. Similarly, the slower component in fluorescence decays from CdS in micelles were assigned to trap states [81] and appeared also wavelength dependent.

After having assigned the fluorescence spectral and decay components, the overall picture is that the variation of the Cd/MSA ratio during aqueous synthesis modulates the size and the surface states of the CdSe QDs by acting on the kinetic rates. Consequently, the emission spectrum of MSA-CdSe QDs is shifted. The Cd/Se ratio may also change both the size and quantum yield of CdSe QDs [82] and the density of surface defects [83], but we kept this ratio constant. Because several parameters intervene, the quantum yield Φ does not strictly follow the QD size. Our results fully agree with the case of 3.0-nm CdTe QDs whose photophysical properties differ according to the synthesis conditions [17,84]. Thus, not only the Cd/Se ratio [83], but also the Cd/thiol ligand ratio during synthesis can change the density of surface defects. It appears that, if the nature of the capping grafted ligand is important, the control of the metal/thiol ligand stoichiometric ratio during QDs synthesis is crucial.

4. Conclusion

The photophysical properties of CdSe QDs stabilized with different thiol ligands crucially depend on the parameters of synthesis in aqueous solution. Whereas the nature of the thiol ligand do not change the QD crystal morphology, it modulates the QD size and the optical characteristics of functionalized CdSe QDs. In the case of MSA used as the thiol capping ligand, a change of the Cd/MSA stoichiometric ratio during aqueous synthesis influences the rate of QDs formation and increased their size, thus directly affecting their photophysics. In particular, the quantum yield, the fluorescence emission spectrum and decays strongly depend on this ratio, which must be carefully monitored when designing QDs for any purpose, especially for probing analytes. Acting on the Cd/MSA ratio appears not only as a mean of modulating the emission spectrum, but also as a mean of understanding the photophysical processes involved with respect to the QD structure.

Supplementary data

Supplementary data related to this article can be found online.

Declaration of interest

The authors declare that they have no competing financial interests.

Acknowledgements

References   [added references in red]

[1]   A.P. Alivisatos, Semiconductor clusters, nanocrystals and quantum dots, Science, 271 (1996) 933–937.

[2]   S.V. Kershaw, A.S. Susha, A.L. Rogach, Narrow bandgap colloidal metal chalcogenide quantum dots: synthetic methods, heterostructures, assemblies, electronic and infrared optical properties, Chem. Soc. Rev. 42 (2013) 3033–3087.

[3]   T. Nann, W.M. Skinner, Quantum dots for electro-optic devices, ACS Nano 5 (2011) 5291–5295.

[4]   T.Y. Zhai, X.S. Fang, L. Li, Y. Bando, D. Golberg, One dimensional CdS nanostructures: synthesis, properties and applications, Nanoscale 2 (2010) 168–187.

[5]   X.Q. Fu, J.Y. Liu, Y.T. Wan, X.M. Zhang, F.L. Meng, J.H. Liu, Preparation of a leaf-like CdS micro-/nanostructure and its enhanced gas-sensing properties for detecting volatile organic compounds, J. Mater. Chem. 22 (2012) 17782–17791.

[6]   R. Freeman, I. Willner, Optical molecular sensing with semiconductor quantum dots (QDs), Chem. Soc. Rev. 41 (2012) 4067–4085.

[7]   X.D. Wang, O.S. Wolfbeis, R.J. Meier, Luminescent probes and sensors for temperature, Chem. Soc. Rev. 42 (2013) 7834–7869.

[8]   V. Rajendran, M. Lehnig, C.M. Niemeyer, Photocatalytic activity of colloidal CdS nanoparticles with different capping ligands, J. Mater. Chem. 19 (2009) 6348–6353.

[9]   K. Zhang, L.J. Guo, Metal sulphide semiconductors for photocatalytic hydrogen production, Catal. Sci. Technol. 3 (2013) 1672–1690.

[10]   R.S. Selinsky, Q. Ding, M.S. Faber, J.C. Wright, S. Jin. Quantum dot nanoscale heterostructures for solar energy conversion, Chem. Soc. Rev. 42 (2013) 2963–2985.

[11]   M. Geszke-Moritz, M. Moritz, Quantum dots as versatile probes in medical sciences: synthesis, modification and properties, Mater. Sci. Eng. C 33 (2013) 1008–1021.

[12]   J. van Embden, J. Jasieniak, P. Mulvaney, Mapping the optical properties of CdSe/CdS heterostructure nanocrystals: the effects of core size and shell thickness, J. Am. Chem. Soc. 131 (2009) 14299–14309.

[13]   T. Torchynska, Y. Vorobiev, Semiconductor II-VI quantum dots with interface states and their biomedical applications, Advanced Biomedical Engineering, Ed. G. Gargiulo Publisher InTech, pp 143–182 (2011).

[14] E.E. Lees, T.-L. Nguyen, A.H.A. Clayton, P. Mulvaney, The preparation of colloidal stable, water-soluble, biocompatible, semiconductor nanocrystals with a small hydrodynamic diameter, ACS Nano 3 (2009) 1121–1182.

[15] J. Jasieniak, P. Mulvaney, From Cd-rich to Se-rich – the manipulation of CdSe nanocrystal surface stoichiometry, J. Am. Chem. Soc. 129 (2007) 2841–2848.

[16] D.A. Hines, P.V. Kamat, Recent advances in quantum dot surface chemistry, ACS Appl. Mater. Interfaces 6 (2014) 3041–3057.

[17] A.L. Rogach, T. Franzl, T.A. Klar, J. Felmann, N. Gaponik, V. Lesnyak, A. Shavel, A. Eychmüller, Y.P. Rakovich, J.F. Dongean, Aqueous synthesis of thiol-capped CdTe nanocrystals: state-of-the-art, J. Phys. Chem. C 111 (2007) 14628–14637.

[18] N. Ben Brahim, M. Poggi, N. Bel-Haj Mohamed, R. Ben Chaâbane, M. Haouari, M. Negrerie, H. Ben Ouada, Synthesis, characterization and spectral temperature-dependence of thioglycerol-CdSe nanocrystals, J. Lumin. 177 (2016) 402–408.

[19] Y. Shirasaki, G.J. Supran, M.G. Bawendi, V. Bulovic, Emergence of colloidal quantum-dot lightemitting technologies, Nature Photonics 7 (2013) 13–23.

[20] K.D. Wegner, N. Hildebrandt, Quantum dots: bright and versatile in vitro and in vivo fluorescence imaging biosensors, Chem. Soc. Rev. 44 (2015) 4792–4834.

[21] M. Yu, G.W. Fernando, R. Li, F. Papadimitrakopoulos, N. Shi, R. Ramprasad, First principles study of CdSe quantum dots: stability, surface unsaturations and experimental validation, Appl. Phys. Lett. 88 (2006) 231910.

[22] E.E. Lees, M.J. Gunzburg, T.-L. Nguyen, G.J. Howlett, J. Rothacker, E.C. Nice, A.H.A. Clayton, P. Mulvaney, Experimental determination of quantum dot size distributions, ligand packing densities, and bioconjugation using analytical centrifugation, Nano Lett. 8 (2008) 2883–2890.

[23] O. Voznyy, S.M. Thon, A.H. Ip, E.H. Sargent, Dynamic trap formation and elimination in colloidal quantum dots, J. Phys. Chem. Lett. 4 (2013) 987–992.

[24] O. Voznyy, E.H. Sargent, Atomistic model of fluorescence intermittency of colloidal quantum dots, Phys. Rev. Lett. 112 (2014) 157401.

[25] S.M. Thon, A.H. Ip, O. Voznyy, L. Levina, K.W. Kemp, G.H. Carey, S. Masala, E.H. Sargent, Role of bond adaptability in the passivation of colloidal quantum dot solids, ACS Nano 7 (2013) 7680–7688.

[26] J.M. Azpiroz, E. Mosconi, J.M. Ugalde, F. De Angelis, Effect of structural dynamics on the opto-electronic properties of bare and hydrated ZnS QDs, J. Phys. Chem. C 118 (2014) 3274–3284.

[27] G. Kalyuzhny, R.W. Murray, Ligand effects on optical properties of CdSe nanocrystals, J. Phys. Chem. B. 109 (2005) 7012–7021.

[28] S. Kilina, S. Ivanov, S. Tretiak, Effect of surface ligands on optical and electronic spectra of semiconductor nanoclusters, J. Am. Chem. Soc. 131 (2009) 7717–7726.

[29] A.M. Munro, I. Jen-La Plante, M.S. Ng, D.S. Ginger, Quantitative study of the effects of surface ligand concentration on CdSe nanocrystal photoluminescence, J. Phys. Chem. C 111 (2007) 6220–6227.

[30] H.H.-Y. Wei, C.M. Evans, B.D. Swartz, A.J. Neukirch, J. Young, O. Prezhdo, T.D. Krauss, Colloidal semiconductor quantum dots with tunable surface composition, Nano Lett. 12 (2012) 4465–4471.

[31] S. Jeong, M. Achermann, J. Nanda, S. Ivanov, V.I. Klimov, J.A. Hollkingsworth, Effect of the thiol–thiolate equilibrium on the photophysical properties of aqueous CdSe/ZnS nanocrystal quantum dots, J. Am. Chem. Soc., 127 (2005) 10126–10127.

[32] N. Ben Brahim, N. Bel-Haj Mohamed, M. Echabaane, M. Haouari, R. Ben Chaâbane, M. Negrerie, H. Ben Ouada, Thioglycerol-functionalized CdSe quantum dots detecting cadmium ions, Sens. Act. B 220 (2015) 1346–1353.

[33] C. Würth, M. Grabolle, J. Pauli, M. Spieles, U. Resch-Genger, Relative and absolute determination of fluorescence quantum yields of transparent samples, Nature Protocols 8 (2013) 1535–1550.

[34] O. Kolmykov, J. Coulon, J. Lalevée, H. Alem, G. Medjahdi, R. Schneider, Aqueous synthesis of highly luminescent glutathione-capped Mn^{2+} doped ZnS quantum dots, Mater. Sci. Eng. C 44 (2014) 17–23.

[35] J.W. Kyobe, E.B. Mubofu, Y.M. Makame, S. Mlowe, N. Revaprasadu, CdSe quantum dots capped with naturally occurring biobased oils, New J. Chem. 39 (2015) 7251.

[36] U. Holzwarth, N. Geibson, The Scherrer equation versus the "Debye-Shcerrer" equation, Nature Nanotech. 6 (2011) 534.

[37] Z. Hens, R.K. Čapek, Size tuning at full yield in the synthesis of colloidal semiconductor nanocrystals, reaction simulations and experimental verification. Coord. Chem. Rev. 263 (2014) 217–228.

[38] R.M. Maceiczyk, L. Bezinge, A.J. deMello, Kinetics of nanocrystal synthesis in a microfluidic reactor: theory and experiment. React. Chem. Eng. 1 (2016) 261–271.

[39] G. Murali, R.D. Amaranatha, P.B. Poorna, R.P. Vijayalakshmi, Structural and optical response of 2-mercaptoethonal capped CdS nanocrystals to Fe^{3+} ions, Cryst. Res. Technol. 47 (2012) 202–206.

[40] L.L. Kazmerski, Polycrystalline and amorphous thin films and devices. Academic press, New York. 1980.

[41] S. Wageh, Raman and photoluminescence study of CdSe nanoparticles capped with a bifunctional molecule, Physica 39 (2007) 8–14.

[42] S.V. Gaponenko, Optical Properties of Semiconductor Nanocrystals Cambridge University press. Cambridge. 1998, 106.

[43] V. Dzhagan, I. Lokteva, C. Himcinschi, X. Jin, J. Kolny-Olesiak, D.R.T. Zahn, Phonon Raman spectra of colloidal CdTe nanocrystals: effect of size, non-stoichiometry and ligand exchange, Nanoscale Res. Letters 6 (2011) 79.

[44] M.J. Fernée, C. Sinito, P. Mulvaney, P. Tamarat, B. Lounis, The optical phonon spectrum of CdSe colloidal quantum dots, Phys. Chem. Chem. Phys., 16 (2014) 16957.

[45] V. Dzhagan, A.G. Milekhin, M. Ya., Valakh, S. Pedetti, M. Tessier, B. Dubertrete, D. R.T. Zahna, Morphology-induced phonon spectra of CdSe/ CdS nanoplatelets: core/shell vs. core–crown, Nanoscale 8 (2016) 17204–17212.

[46] A.M. Chaparro, M.A. Martinez, C. Guillen, R. Bayon, M.T. Gutierrez, J. Herrero, SnO_2 substrate effects on the morphology and composition of chemical bath deposited ZnSe thin films, Thin Solid Films 361 (2000) 177–182.

[48] A.M. Kelley, Electron–phonon coupling in CdSe nanocrystals from an atomistic phonon model, ACS Nano 7 (2011) 5254–5262.

[49] E.S.F. Neto, N.O. Dantas, S.W. da Silva, P.C. Morias, M.A.P. da Silva, Confirming the lattice contraction in CdSe nanocrystals grown in a glass matrix by Raman scattering, J. Raman Spectrosc. 41 (2010) 1302–1305.

[50] S.K. Islam, M.A. Sohel, J.R. Lombardi, Coupled exciton and charge transfer resonances in the Raman enhancement of phonon modes of CdSe quantum dots, J. Phys. Chem. C. 118 (2014) 19415–19421.

[51] M. Kosmulski, pH-dependent surface charging and points of zero charge III. update, J Colloid Interface Sci. 298 (2006) 730–741.

[52] T. Imae, K. Muto, S. Ikeda, The pH dependence of dispersion of TiO_2 particles in aqueous surfactant solutions, Colloid Polym. Sci. 269 (1991) 43–48.

[53] K.Y. Cai, M. Frant, J. Bossert, G. Hildbrand, K. Liefeith, K.D. Jandt, Surface functionalized titanium thin films: zeta potential, protein adsorption and cell proliferation, Colloids Surf. B: Biointerfaces 50 (2006) 1–8.

[54] P. Attard, D. Antelmi, I. Larson, Comparison of the zeta potential with the diffuse layer potential from charge titration, Langmuir 16 (2000) 1542–1552.

[55] M. Erdemoglu, M. Sarikaya, Effects of heavy metals and oxalate on the zeta potential of magnetite, J. Colloid Interface Sci. 300 (2006) 795–804.

[56] R. Eriksson, J. Merta, J. Rosenholm, The calcite/water interface II. Effect of added lattice ions on the charge properties and adsorption of sodium polyacrylate, J. Colloid Interface Sci. 326 (2008) 396–402.

[57] P. Wang, A.A. Keller, Nature and engineered nano and colloidal transport: role of zeta potential and prediction of particle deposition, Langmuir 25 (2009) 6856–6862.

[58] L.E. Brus, Electron–electron and electron–hole interactions in small semiconductor crystallites: The size dependence of the lowest excited electronic state, J. Chem. Phys. 80 (1984) 4403–4409.

[59] M. Tamborra, M. Striccoli, R. Comparelli, M.L. Curri, A. Petrella, A. Agostiano, Optical properties of hybrid composites based on highly luminescent CdS nanocrystals in polymer, Nanotechnol. 15 (2004) 240–244.

[60] W.W. Yu, L.H. Qu, W.Z. Guo, X.G. Peng, Experimental determination of the extinction coefficient of CdTe, CdSe, and CdS nanocrystals, Chem. Mater. 15 (2003) 2854–2860.

[61] N. Ben Brahim, M. Poggi, J.-C. Lambry, N. Bel Haj Mohamed, R. Ben Chaâbane, M. Negrerie, Density of grafted chains in thioglycerol-capped CdS quantum dots determines their interaction with aluminium(III) in water, Inorg. Chem. 57 (2018) 4979–4988.

[62] N. Ben Brahim, N. Bel-Haj Mohamed, M. Poggi, R. Ben Chaâbane, M. Haouari, H. Ben Ouada, M. Negrerie, Interaction of L-cysteine functionalized CdSe quantum dots with metallic cations and selective binding of cobalt in water probed by fluorescence, Sens. Act. B 243 (2017) 489–499.

[63] N. Bel Haj Mohamed, N. Ben Brahim, R. Mrad, M. Haouari, R. Ben Chaâbane, M. Negrerie, Use of MPA-capped CdS quantum dots for sensitive detection and quantification of Co^{2+} ions in aqueous solution, Anal. Chim. Acta 1028 (2018) 50–58.

[64] J. Jasieniak, L. Smith, J. van Embden, P. Mulvaney, Re-examination of the size-dependent absorption properties of CdSe quantum dots, J. Phys. Chem. C 113 (2009) 19468–19474.

[65] Y.H. Zhang, H.S. Zhang, M. Ma, X.F. Guo, H. Wang, The influence of ligands on the preparation and optical properties of water-soluble CdTe quantum dots, Appl. Surf. Sci. 255 (2009) 4747–4753.

[66] A. Kumari, R.R. Singh, Encapsulation of highly confined CdSe quantum dots for defect free luminescnce and improved stability, Physica E 89 (2017) 77–85.

[67] L. Jethi, T.G. Mack, M.M. Kraus, S. Drake, P. Kambhampati, The effect of exciton-delocalizing thiols on intrinsic dual emitting semiconductor nanocrystals, Chem. Phys. Chem. 17 (2016) 665–699.

[68] A.D. Dukes, M.A. Schreuder, J.A. Sammons, J.R. McBride, N.J. Smith, S.J. Rosenthal, Pinned emission from ultrasmall cadmium selenide nanocrystals, J. Chem. Phys. 129 (2008) 121102.

[69] H. Sharma, S.N. Sharma, G. Singh, S.M. Shivaprasad, Effect of ratios of Cd:Se in CdSe nanoparticles on optical edge shifts and photoluminescence properties, Physica E 31 (2006) 180–186.

[70] A.R. Kortan, R. Hull, R.L. Opila, M.G. Bawendi, M.L. Steigerwald, P.J. Carroll, L.E. Brus, Nucleation and growth of CdSe on ZnS quantum crystallite seeds and vice versa, in inverse micelle media, J. Am. Chem. Soc. 112 (1990) 1327–1332.

[71] A.C.A. Silva, S.L. Vieira de Deus, M.J.B. Silva, N.O. Dantas, Highly stable luminescence of CdSe magic-sized quantum dots in Hela cells, Sens. Act. B 191 (2014) 108–114.

[72] D.R. Baker, P.V. Kamat, Tuning the emission of CdSe quantum dots by controlled trap enhancement, Langmuir 26 (2010) 11272–11276.

[73] N. Pinna, K. Weiss, J. Urban, M.-P. Pileni, Triangular CdS nanocrystals: structural and optical studies, Adv. Mater. 13 (2001) 261–264.

[74] D. Samanta, B. Samanta, A.K. Chaudhuri, K. Ghorai, U. Pal, Electrical characterization of stable air-oxidized CdSe films prepared by thermal evaporation, Semicond. Sci. Technol. 11 (1996) 548–553.

[75] A. Veamatahau, B. Jiang, T. Seifert, S. Makuta, K. Latham, M. Kanehara, T. Teranishi, Y. Tachibana, Origin of surface trap states in CdS quantum dots: relationship between size dependent photoluminescence and sulfur vacancy trap states, Phys. Chem. Chem. Phys. 17 (2015) 2850–2858.

[76] I.-S. Liu, H.-H. Lo, C.-T. Chien, Y.-Y. Lin, C.-W. Chen, Y.-F. Chen, W.-F. Su, S.-C. Liou, Enhancing photoluminescence quenching and photoelectric properties of CdSe quantum dots with hole accepting ligands, J. Mater. Chem. 18 (2008) 675–682.

[77] H. Zhang, D.Y. Wang, H. Mohwald, Ligand-selective aqueous synthesis of one-dimensional CdTe nanostructures, Angew. Chem. Int. Ed. 45 (2006) 748–751.

[78] D. Zhou, J.S. Han, Y. Liu, M. Liu, X. Zhang, H. Zhang, B. Yang, Nucleation of aqueous semiconductor nanocrystals: a neglected factor for determining the photoluminescence, J. Phys. Chem. C 114 (2010) 22487–22492.

[79] R.R. Cooney, S.L. Sewall, E.A. Dias, D.M. Sagar, K.E.H. Anderson, P. Kambhampati, Unified picture of electron and hole relaxation pathways in semiconductor quantum dots, Phys. Rev. B. 75 (2007) 245311.

[80] J. Zhang, X. Zhang, J.Y. Zhang, Size-dependent time-resolved photoluminescence of colloidal CdSe nanocrytals, J. Phys. Chem. 113 (2009) 9512–9515.

[81] Y. Ding, S.Z. Shen, H. Sun, K. Sun, F. Liu, Synthesis of L-glutathione-capped ZnSe quantum dots for the sensitive determination of copper ion in aqueous solutions, Sens. Act. B 203 (2014) 35–43.

[82] C.W. Wang, M.G. Moffit, Surface-tunable photoluminescence from block copolymer-stabilized cadmium sulfide quantum dots, Langmuir, 20 (2004) 11784–11796.

[82] X.Y. Wang, L.H. Qu, J.Y. Zhang, X.G. Peng, Xiao, M. Surface-related emission in highly luminescent CdSe quantum dots, Nano Lett. 3 (2003) 1103–1106.

[83] A.C.A. Silva, M.J.B. Silva, F.A. Cordero da Luz, D. Pereira Silva, S.L. Vieira de Deus, N.O. Dantas, Controlling the cytotoxicity of CdSe magic-sized quantum dots as a function of surface defect density, Nano Lett. 14 (2014) 5452–5457.

[84] M.Y. Gao, S. Kirstein, H. Möhwald, A.L. Rogach, A. Kornowski, A. Eychmüller, H. Weller, Strongly photoluminescent CdTe nanocrystals by proper surface modification, J. Phys. Chem. B 102 (1998) 8360–8363.